Dynamics Properties of Photosynthetic Microorganisms Probed by Incoherent Neutron Scattering

Daniela Russo, Maya Dimova Lambreva, Christiane Alba-Simionesco, Pierre Sebban, Giuseppina Rea

Please cite this article in press as: Russo et al., Dynamics Properties of Photosynthetic Microorganisms Probed by Incoherent Neutron Scattering, Biophysical Journal (2019), https://doi.org/10.1016/j.bpj.2019.03.029

Biophysical *Journal*
Article

Biophysical Society

Dynamics Properties of Photosynthetic Microorganisms Probed by Incoherent Neutron Scattering

Daniela Russo,[1,2,*] Maya Dimova Lambreva,[3] Christiane Alba Simionesco,[4] Pierre Sebban,[5] and Giuseppina Rea[3]

[1]CNR Istituto Officina Materiali, Institut Laue-Langevin, Grenoble, France; [2]Institut Lumière Matière, UMR5306 Université Claude Bernard Lyon 1 et CNRS, Villeurbanne, France; [3]CNR Istituto di Cristallografia, Monterotondo Stazione, Rome, Italy; [4]Laboratoire Leon Brillouin (CEA/CNRS), CEA Saclay, Gif-sur Yvette Cedex, France; and [5]Laboratoire de Chimie Physique, Université Paris Sud, Orsay, France

ABSTRACT Studies on the dynamical properties of photosynthetic membranes of land plants and purple bacteria have been previously performed by neutron spectroscopy, revealing a tight coupling between specific photochemical reactions and macromolecular dynamics. Here, we probed the intrinsic dynamics of biotechnologically useful mutants of the green alga *Chlamydomonas reinhardtii* by incoherent neutron scattering coupled with prompt chlorophyll fluorescence experiments. We brought to light that single amino acid replacements in the plastoquinone (PQ)-binding niche of the photosystem II D1 protein impair electron transport (ET) efficiency between quinones and confer increased flexibility to the host membranes, expanding to the entire cells. Hence, a more flexible environment in the PQ-binding niche has been associated to a less efficient ET. A similar function/dynamics relationship was also demonstrated in *Rhodobacter sphaeroides* reaction centers having inhibited ET, indicating that flexibility at the quinones region plays a crucial role in evolutionarily distant organisms. Instead, a different functional/dynamical correlation was observed in algal mutants hosting a single amino acid replacement residing in a D1 domain far from the PQ-binding niche. Noteworthy, this mutant displayed the highest degree of flexibility, and besides having a nativelike ET efficiency in physiological conditions, it acquired novel, to our knowledge, phenotypic traits enabling it to preserve a high maximal quantum yield of photosystem II photochemistry in extreme habitats. Overall, in the nanosecond timescale, the degree of the observed flexibility is related to the mutation site; in the picosecond timescale, we highlighted the presence of a more pronounced dynamic heterogeneity in all mutants compared to the native cells, which could be related to a marked chemically heterogeneous environment.

INTRODUCTION

The dynamical properties of biomolecules inside a living cell contribute to define its intrinsic functionality and/or adaptation to the environment. In this regard, dynamic neutron scattering is the most direct experimental technique to investigate the internal dynamics of biological systems (1,2). Because of their inherent wavelength (≈ ångström) and energy (≈ milli electronvolt), neutrons are specifically suited to measure self and collective motions on picosecond-microsecond timescales matching the amplitude and frequency of molecular motions in biomolecules. Furthermore, because neutrons are distinctively sensitive to hydrogen and its isotopes, neutron scattering measurements enable the study of simple as well as complex biological systems that can be labeled by deuterium (3). Specifically, incoherent neutron scattering techniques are used to probe the intrinsic dynamics of key proteins isolated from evolutionarily distant organisms and to highlight the relevance of hydration water in protein function (4–9). Likewise, incoherent neutron scattering was successfully applied to investigate diffusive and vibrational motions even in more complex intracellular biosystems (e.g., the photosynthetic membranes of land plants and bacteria), providing evidence that dynamics properties contribute to define functional properties even in the highly specialized membranes hosting the components of the photosynthetic electron transport (ET) chain (10–15).

The photosynthetic apparatus is a large assembly of pigment-protein complexes converting solar energy into chemical energy through a series of ET reactions. It contains, among others, PSII-type core catalytic domain, embedded in thylakoid membranes (TMs) and made by the reaction center (RC) protein heterodimer D1/D2 (in

Submitted December 13, 2018, and accepted for publication March 20, 2019.

*Correspondence: russo@ill.fr

Editor: Jill Trewhella.

https://doi.org/10.1016/j.bpj.2019.03.029

Please cite this article in press as: Russo et al., Dynamics Properties of Photosynthetic Microorganisms Probed by Incoherent Neutron Scattering, Biophysical Journal (2019), https://doi.org/10.1016/j.bpj.2019.03.029

oxygenic phototrophs such as *Chlamydomonas reinhardtii*) or the orthologous proteins L/M (in anoxygenic purple bacteria such as *Rhodobacter sphaeroides*) (16). These heterodimers, known as type II RCs, use quinones as electron acceptors and are characterized by three-dimensional structure conservation and cofactors arrangement, which guarantee efficient-forward ET (17).

After light absorption by antenna complexes, special (bacterio) chlorophylls in the RCs transfer electronic excitation energy along several cofactors leading to charge separation. At the acceptor site of both RCs, the one-electron acceptor quinone Q_A is reduced to Q_A^- in ~400 ps by the primary electron carrier intermediate pheophytin. Subsequently, in 200–400 μs, the Q_A^- reduces the nearest two-electron carrier quinone Q_B to Q_B^- in a conformationally gated process possibly involving hydrogen bond (H-bond) remodeling. After accepting two electrons and two protons, Q_B^- is converted to quinol QH_2 and released from the quinone-binding niche shaped by specific domains of the D1 or L proteins (18–20). The Q_B quinones can be displaced by chemically different competitive inhibitors impairing the photosynthetic ET chain. These inhibitors include specific classes of herbicides (e.g., triazines) that were used to deepen the understanding of the photochemical events (21) and then to support the development of photosynthesis-based biosensors for environmental monitoring (22–24).

A critical mass of experimental, theoretical, and in silico studies has already made a significant impact in understanding the thermodynamic and kinetic aspects of photoinduced energy and ET processes and has also started to highlight a close coupling between RC dynamics and reactivity. Notably, it was shown that in physiological conditions, the kinetics of charge separation and ET processes are controlled by a complex conformational dynamics covering a wide range of timescales, relying on the RC's capability to fluctuate among a large number of nearly isoenergetic conformational substates (13,25,26). Hence, any perturbations of the native RC flexibility can potentially interfere with its biological function. In this regard, elastic incoherent and quasielastic neutron scattering (*EINS* and *QENS*) experiments performed on wild-type (WT) PSII-enriched membranes revealed the onset of diffusive protein motions at the same temperature and hydration levels promoting an increase of the efficiency of ET from Q_A^- to Q_B, and a reduction of the membrane's flexibility in samples in which the ET efficiency from Q_A^- to Q_B was transiently inhibited by a saturating laser flash (11–14). Furthermore, *EINS* studies probed an increased membrane flexibility at physiological temperatures above 310 K that was associated to the inactivation of the oxygen-evolving complex (15). In purple bacteria RCs, *QENS* measurements demonstrated that two photosynthetically nonactive site-specific mutants of the L subunit have a more flexible core compared to that of the functional WT (10).

In this study, *EINS* and *QENS* experiments, combined to prompt chlorophyll fluorescence measurements, have been performed to investigate whether single point mutations in the crucial D1 protein of *C. reinhardtii* confer novel, to our knowledge, dynamic properties to the entire algal cells and isolated thylakoids and if the intrinsic dynamics is correlated to protein activity or function. Overall, the results indicate that specific amino acids residing in the plastoquinone (PQ)-binding niche are essential for preserving the functional protein flexibility and that a generally more rigid environment supports efficient ET from Q_A to Q_B.

MATERIALS AND METHODS

Strains and growth conditions

Chlamydomonas strains were grown photoheterotrophically in Tris-acetate-phosphate (TAP) medium (pH 7.2) (27) in Erlenmeyer flasks at 24°C under continuous illumination (50 μmol photons $m^{-2}s^{-1}$) and constant shaking (150 rpm). In all analyses, cells from algal cultures in late exponential growth phase (~4–5 $\times$ 10^6 cell mL^{-1}) were harvested by 5-min centrifugation at 20°C and 2500 rpm and further processed for different purposes.

Chlorophyll a fluorescence analysis

Before cell harvesting, the photosynthetic performance of *Chlamydomonas* cultures was evaluated by registering the chlorophyll *a* fluorescence induction curves at 24°C in TAP medium by the Plant Efficiency Analyzer (Hansatech Instruments, Norfolk, UK) (28). The maximal quantum yield of PSII photochemistry was calculated as $F_v/F_m = (F_m - F_0)/F_m$; the efficiency of the ET between PSII primary (Q_A) and secondary (Q_B) quinone electron acceptors was evaluated by the parameter $1-V_J$, where $1-V_J = 1 - [(F_{2\ ms} - F_0)/(F_m - F_0)]$. F_0, F_m and $F_{2\ ms}$ are the fluorescence level at 50 μs, the maximal fluorescence, and the fluorescence level at 2 ms after the onset of the illumination, respectively. The measurements were performed at least three times on each culture (28).

Preparation of cells and thylakoids for neutron exposure

In these experiments, we considered hydrogenated *Chlamydomonas* strains. To replace the intracellular H_2O with D_2O, algal cultures were centrifuged at 4000 rpm and at 4°C for 30 min, and the cell pellets were washed with deuterated TAP medium. The operation was repeated twice. We estimated that the intercellular water was also removed from the cell pellet.

Algal photosynthetic membranes, namely thylakoids, were isolated as previously reported (29), with modifications as described in Supporting Materials and Methods.

About 1 g of *C. reinhardtii* cell pellet or thylakoid extracts was used for each exposure to neutrons.

The sample water content was previously surveyed in an independent experiment by weighing the dry and wet mass before and after baking the pellets at 75°C for 48 h. Water constituted ~80% of the total cell weight. The choice of heavy water guarantees that almost all the scattered intensity results from the interaction of neutrons, with the hydrogen atoms located on the biomolecules side because of their very large incoherent cross section.

EINS and *QENS*

The *EINS* measurements were performed on the backscattering spectrometer IN16 at the Institut Laue-Langevin (ILL) (Grenoble, France) with an

Please cite this article in press as: Russo et al., Dynamics Properties of Photosynthetic Microorganisms Probed by Incoherent Neutron Scattering, Biophysical Journal (2019), https://doi.org/10.1016/j.bpj.2019.03.029

energy resolution of 1 μeV (that corresponds to a timescale of the order of 650 ps) in a range of temperature between 50 and 300 K. The spectrometer was set in the operational elastic mode (i.e., the Doppler speed of the monochromator was set equal to zero), and the collected signal was measured over a wave vector Q range extending from 0.2 to 1.89 Å^{-1} (where $Q = 4\pi\sin\theta/\lambda$ is the elastic momentum exchange, 2θ is the scattering angle, and λ is the wavelength of the incident neutrons). All the elastic scans, performed as a function of temperature, were recorded using a heating rate of 0.5 K/min and an acquisition time equal to 3 min per point. A typical elastic scan collection time was of the order of 8 h per sample. The *QENS* measurements were performed on the IN6 time-of-flight spectrometer at ILL. The experiment was carried out using an incident neutron wavelength λ = 5.1 Å^{-1}, corresponding to a full-width energy resolution of 70 μeV, and a wave vector range of 0.3–2.0 Å^{-1}.

For each measurement, we layered fresh algae cell paste into a 0.5-mm thick standard flat aluminum sample holder. Four biological replicates were analyzed as a function of temperature. All spectra were corrected for detector efficiencies and normalized to their 20 K temperature scans (*EINS*) or standard vanadium (*QENS*), using the ILL LAMP programs (information on the program is available on the ILL website at http://www.ill.fr). The resulting data have been analyzed with DAVE program (https://www.ncnr.nist.gov/dave/index.html).

Mean-square displacement (MSD), diffusive properties, and relaxation times were investigated in the picosecond timescale. A description of the analysis strategy is provided in Supporting Materials and Methods.

RESULTS AND DISCUSSION

Description and photochemical performance of the PSII D1 mutants

Function/dynamics studies on photosynthetic eukaryotic cells stably hindered in the ET processes have not been reported yet. In this framework, the availability of a large repertoire of D1 mutants of the unicellular green alga *C. reinhardtii*, a deeply explored model system for fundamental, and applied research represents a valuable tool (30,31).

In our previous studies, molecular docking techniques and molecular dynamic simulations guided the design of site-directed mutants of *C. reinhardtii* with improved affinity for specific classes of herbicides, revealing that, among others, mutations of the D1-Phe265 (F265) residue can stabilize the atrazine docking in the electron acceptor Q_B-binding pocket (30,32). On the contrary, site-directed mutations of the D1-Ser264 (S264) led to the production of algal strains resistant to atrazine having impaired binding of either the natural Q_B ligand or Q_B analogs (i.e., triazine herbicides) according to the literature (30,33–35). Finally, by combining an evolution strategy directed in vitro followed by site-directed mutagenesis, we isolated D1-Ile163 (I163) mutants having improved tolerance to extreme environmental conditions (30,36,37).

To deepen the knowledge on the function/dynamics relationships occurring in photosynthetic redox-active sites, we probed by *EINS* and *QENS* the dynamics properties of the I163N-, S264K-, and F265T-mutated strains (31–34) in comparison with the *C. reinhardtii* intronless (IL) genotype (38).

The I163 amino acid resides in the transmembrane helix III of the D1 protein exposed toward the stromal site, and it is included in the environment of the redox-active Tyr Z conducting the water oxidation. The S264 and F265 amino acids are hosted in the loop connecting the transmembrane helices IV and V of the D1 protein and contribute to shape the Q_B-binding niche (21,39) (Fig. S1; Table S1). Before exposing the cells to neutrons, the photochemical performance of the cultures was assessed by monitoring the chlorophyll *a* fluorescence parameters (Table 1). Values reported in Table 1 indicate that in the S264K and F265T mutants, the efficiency of the ET ($1-Vj$) was severely affected, whereas the maximal quantum yield of PSII photochemical reaction (F_v/F_m) was poorly influenced. Hence, the introduced amino-acidic substitution produced viable and photosynthetic active mutants having a reduction of the ET efficiency, however. Indeed, previous bioinformatic experiments performed in these mutants revealed a remodeling of the H-bond network occurring in the PQ-binding niche leading to a reduced capability to interact with the natural Q_B cofactor or the competitive inhibitor herbicides, thus impairing ET (34,35).

On the other end, the I163N mutant, which behaves as a radiation-tolerant strain upon exposure to ionizing and fluxes either in on-ground experiments or in low-earth orbit space flight (36,37), shared a photochemical performance similar to the native IL genotype (Table 1). A computational analysis attributed the basis of this improved phenotype to the formation of a more stable complex through the establishment of more productive contacts of the more hydrophilic side chain of N163 with neighboring D1 and D2 amino acids and chloroplast membrane lipid components compared to the WT I163 (37).

EINS

The *EINS* intensity arises from atoms, which are immobile on the timescale of the instrumental resolution, and provides information on the average size of the space occupied by the movements of hydrogen atoms. Here, the elastic scattering profile of hydrogenated cells washed and suspended in D_2O-based medium has been measured as a function of temperature in the range 50–300 K. Fig. 1 reports the elastic

TABLE 1 Description of the Main Features of the Analyzed Mutants

	F_v/F_m	$1-V_J$	Main Phenotypic Traits
IL	0.805 ± 0.007	0.571 ± 0.006	nativelike
I163N	0.793 ± 0.013	0.560 ± 0.011	tolerance to ionizing radiation (36,37)
S264K	0.748 ± 0.010	0.241 ± 0.017	resistance to the s-triazine herbicides (33,65)
F265T	0.724 ± 0.010	0.239 ± 0.013	sensitivity to atrazine (30,32)

s-triazine herbicides include atrazine, simazine, ametryne, prometryn, and prometon (30,33,66).

Please cite this article in press as: Russo et al., Dynamics Properties of Photosynthetic Microorganisms Probed by Incoherent Neutron Scattering, Biophysical Journal (2019), https://doi.org/10.1016/j.bpj.2019.03.029

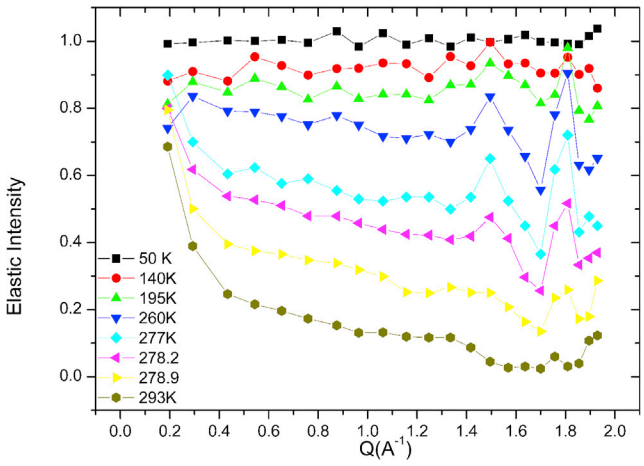

FIGURE 1 Elastic intensity as a function of wave vector Q ($Å^{-1}$) and temperature (low T to high T = *top* to *bottom*) for the native green algae. The observed peaks at 1.5 and 1.8 $Å^{-1}$ are associated to the hexagonal ice formation at low temperature. To see this figure in color, go online.

intensity as a function of wave vector Q ($Å^{-1}$) and temperature (low T to high T = *top to bottom*) for the native green algae (examples for mutants are provided in Fig. S2). The observed Bragg peaks at 1.5 and 1.8 $Å^{-1}$ are the hexagonal ice's fingerprints. The temperature dependence of the peak's intensity suggested that the ice fully melts at 279 K.

Because the ice formation could damage the cells during the cooling/heating process, we compared these measurements with those performed in the physiological range (280–300 K) before cooling. Nevertheless, a complete measurement in the range of temperature between 50 and 300 K allowed data normalization using low-temperature data (50 K), giving access to the vibrational fluctuations.

Fig. 2 shows the integrated elastic intensities (summed in the range 0.4 and 1.42 $Å^{-1}$ to avoid the water Bragg peak

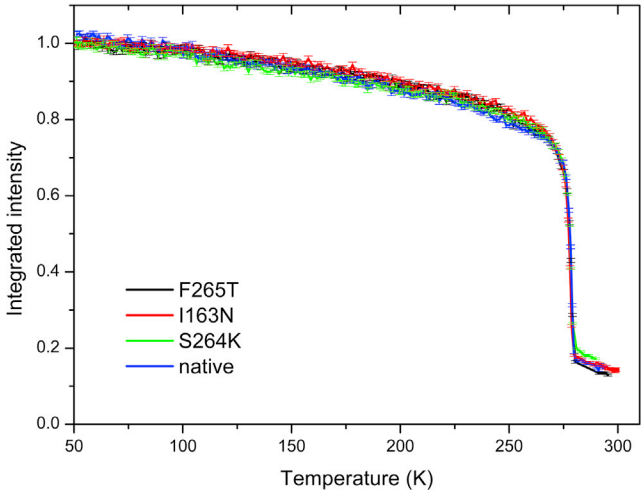

FIGURE 2 Integrated elastic intensities (summed in the range 0.4 and 1.42 $Å^{-1}$) as a function of temperature for native *Chlamydomonas* and D1 mutants I163N, S264K, and F265T. To see this figure in color, go online.

region) as a function of temperature for native and mutated *Chlamydomonas* cells. Error bars are represented for all curves, exhibiting the same general trend. The common smooth decrease of the elastic line followed by an abrupt drop of the integrated intensity confirmed the presence of ice for all samples. The continuous decrease of intensity is due to the increasing amplitude of molecular vibrations, whereas the larger slope is representative of a significant change of dynamics in the sample (here represented by the melting of the intracellular water).

Regrettably, the integrated intensities, which usually provide preliminary information (40,41), were not informative enough to compare the dynamics of mutants; hence, to get insights in the flexibility of the cells, we have extrapolated the corresponding MSDs reporting the <u2>/3 values (see Supporting Materials and Methods). Fig. 3 represents the MSDs extracted in the Q^2 range 0.15–1.96 $Å^{-2}$.

Up to the melting transition, all the atomic/molecular vibrations are identical within error bars. All atoms constrained in a rigid matrix, such as the ice, can vibrate without diffusion, giving access to the Debye-Waller. The first-order

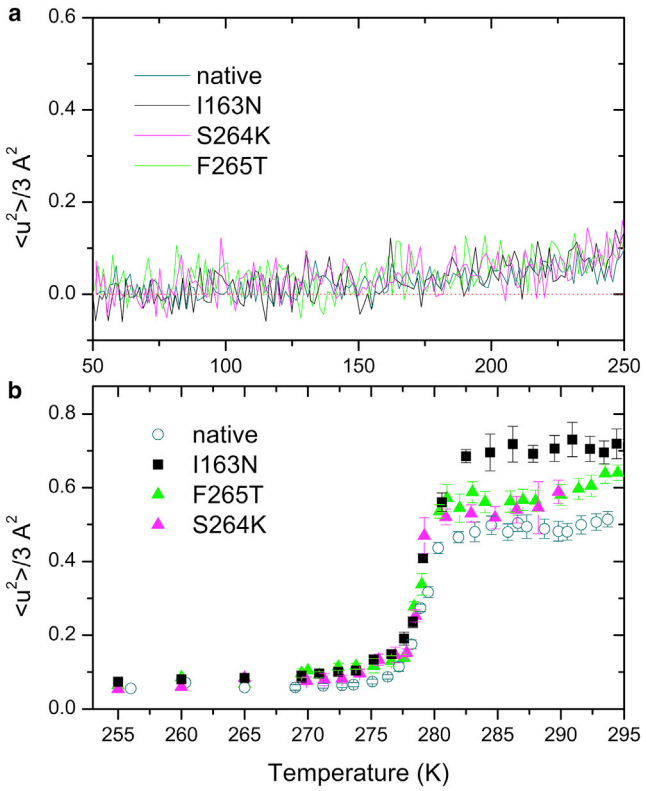

FIGURE 3 Mean-square displacement (MSD) as a function of temperature for native *Chlamydomonas* and D1 mutants I163N, S264K and F265T. (*a*) A low range of temperature (50–250 K) below the ice melting temperature is shown. In this range, only harmonic motions are observed. (*b*) A range of temperature from ice melting up to physiological temperature (255–295 K) is shown. At the physiological temperatures, the MSDs associated to mutants are higher than the native cell. To see this figure in color, go online.

Please cite this article in press as: Russo et al., Dynamics Properties of Photosynthetic Microorganisms Probed by Incoherent Neutron Scattering, Biophysical Journal (2019), https://doi.org/10.1016/j.bpj.2019.03.029

transition (solid-liquid) occurred for all samples in the same very narrow range of temperature (276–280 K). For the temperature above 280 K, the MSDs were relatively independent on temperature and showed distinct amplitudes between native and mutant strains. The trend highlights that the green algal cells carrying genetic mutations have, in general, higher MSD amplitudes compared to the native cells (Fig. S3). This behavior indicates that at the physiological temperatures, mutants are more flexible than the native algae. In particular, F265T and S264K mutants, which carry the single point mutation in the stromal DE loop hosting the Q_B-binding site (Fig. S1; Table S1), showed similar amplitude of the MSD. Instead, the I163N mutant, where the mutation resides in the transmembrane helix C toward the luminal side outside the PQ-binding niche, revealed a well-distinct and enhanced MSD value. It is important to note that by analyzing the mutants directly at the physiological range of temperature, we measured the same dynamics and observed the same trend among mutants we described above (Fig. 4). This allowed us to rule out the hypothesis that the observed differences were due to possible damages occurring as a consequence of low-temperature exposure (Fig. S4).

To better understand the origin of this change on flexibility, we measured the MSD of TMs isolated from the native and F265T strains (see Supporting Materials and Methods). Fig. 5 a shows the MSDs values of the native and F265T TM in the physiological range of temperature 280–298 K. We found a consistency with the results reported in Fig. 3 for the whole *Chlamydomonas* cells. The MSD values had distinct amplitude up to 292 K, then thermal fluctuations dominated and smoothed all differences. The TMs of the modified organism were more flexible than those of the native organism; it is tempting to speculate that some of this lack of rigidity directly arises from the

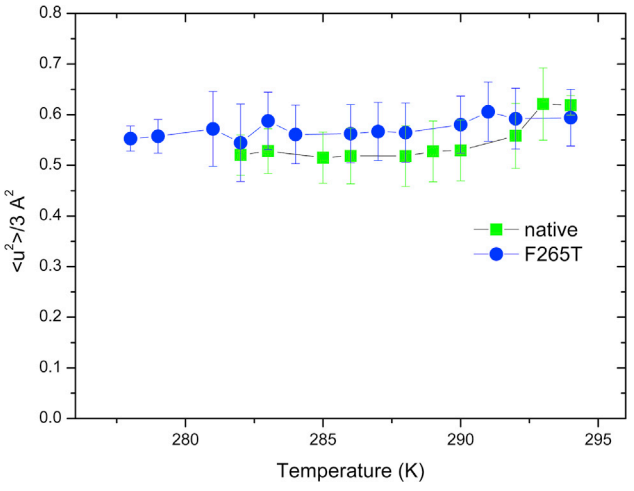

FIGURE 4 Mean-square displacement (MSD) of the native and the F265T green algae measured as a function of temperature before cooling in the range of temperature 277–300 K. To see this figure in color, go online.

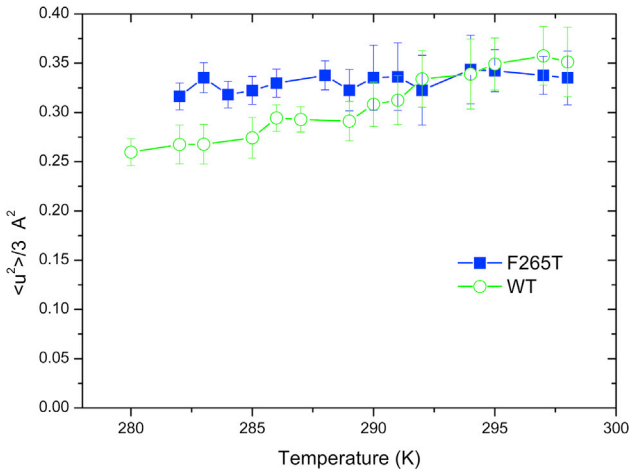

FIGURE 5 Mean-square displacement (MSD) in the TM of the native and F265T green algae measured as a function of temperature before cooling in the range of temperature 280–300 K. To see this figure in color, go online.

mutated PSII D1 protein. By comparing the *Chlamydomonas* TM and whole-cell dynamics (Fig. 6), we observed that the TMs have higher MSD amplitudes, which led us to hypothesize that the major contribution to the whole-cell flexibility is provided by these extended protein-lipid

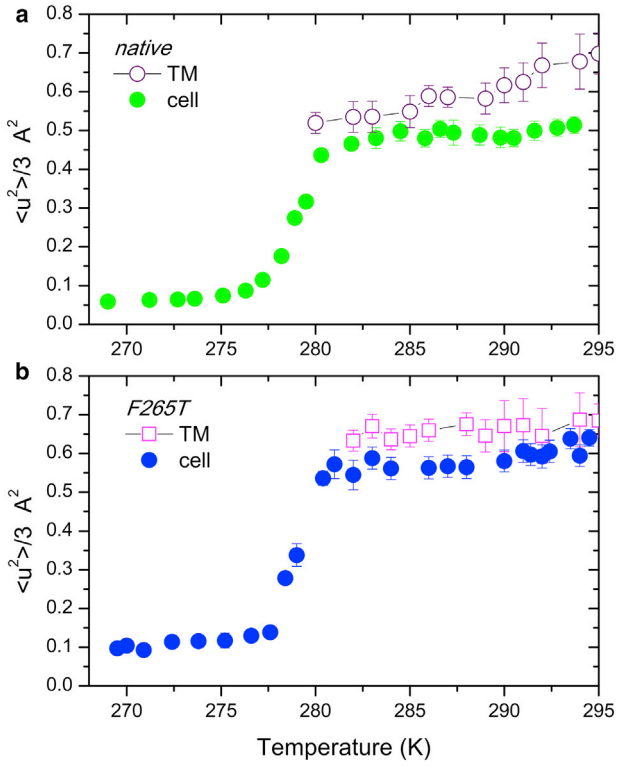

FIGURE 6 MSDs of the *Chlamydomonas* TM and the whole cell for the native (*a*) and the F265T strains (*b*). TMs have higher MSDs amplitudes, indicating the major contribution to the whole-cell flexibility. To see this figure in color, go online.

Please cite this article in press as: Russo et al., Dynamics Properties of Photosynthetic Microorganisms Probed by Incoherent Neutron Scattering, Biophysical Journal (2019), https://doi.org/10.1016/j.bpj.2019.03.029

systems including all the macromolecular assemblies involved in the light reactions of photosynthesis. In this context, it is interesting to note that the I163N mutant has a larger flexibility compared to the other mutants and that this dynamical behavior does not correlate to ET efficiency, possibly because of the fact that the mutation is located in a D1 domain far from the PQ-binding site. Most probably, the larger flexibility assumed by the mutant and its environment could be related to its ability to tolerate stress conditions as it has been already observed in completely different species (3,42,43). On the contrary, the increased flexibility observed in the S264K and F265T mutants is associated to the attenuated photosynthetic ET efficiency and, at least for S264K, also a reduction of the oxygen evolution rate (35).

Changes in the dynamics arising from the genetic manipulation of photosynthetic RC were also observed in the purple bacterium *R. sphaeroides*, hosting mutations in the D1-D2 orthologous proteins L/M. Here, the introduced mutations led to a ~1000 times reduction of proton transfers to Q_B, giving rise to mutants unable to perform photosynthesis (10). In this context, it was demonstrated that the native RC is globally more rigid than the nonfunctional mutant. Therefore, with the help of Brownian dynamics simulation, the authors claimed that the requirement of a rigid core is necessary to accomplish the RC protein function. Here, we confirmed the functional/rigidity hypothesis by measuring the elastic scattering of RCs trapped in their active and inactive states, namely by freezing them under light or dark conditions, respectively. Previous studies revealed that in RCs frozen under light, the ET from Q_A^- to Q_B occurs efficiently even at the cryogenic temperature of 50 K, whereas in RCs frozen in the dark, this reaction slows with temperature and stops below 200 K. These observations were interpreted with the existence of different active conformational substates occurring and trapped in the light condition, enabling the reduction of Q_B (25,26). In our experiments, the RCs cooled under continuous high illumination (details in Supporting Materials and Methods) revealed a different temperature dependence of the MSD compared to the RCs cooled in the dark (Fig. 7). Specifically, in the region 120–220 K, the light-adapted samples showed a higher rigidity compared to the dark-adapted ones. This behavior is of particular biological relevance because in this temperature range, RCs undergo relaxation processes giving rise to the coexistence of active and inactive conformational substates separated by small energy barriers (25,26). We, hence, strengthen our hypothesis that in purple bacteria RCs, a more rigid core leads to a more efficient Q_A^- to Q_B ET.

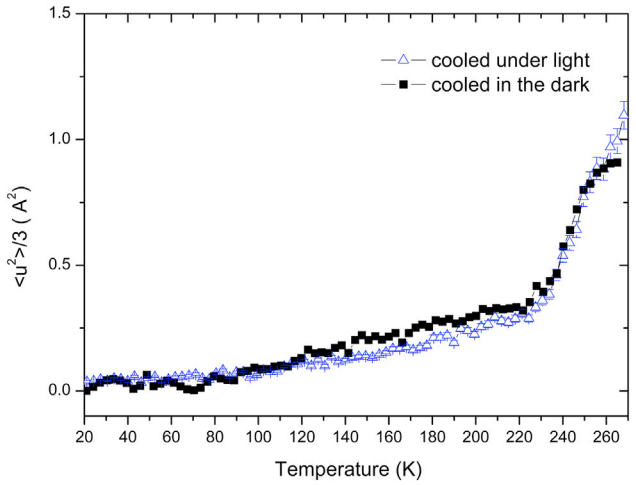

FIGURE 7 MSDs of the *R. sphaeroides* reaction center (RC) cooled under light and in the dark. It is possible to remark a slight variation of the MSD slope as a function of the cooling method. The higher the slope is, the more flexible the system is. To see this figure in color, go online.

QENS

The *QENS* intensity arises from atoms, which exchange only small energy, and gives information on diffusive and relaxation times properties providing insights into local dynamics. To quantify the relaxation time at room temperature, we hence measured the *QENS* spectrum probing the local dynamics in the picosecond timescale, providing also time parameters and characteristic lengths. The goal was to investigate to which extent the internal molecular dynamics measured for the entire cell, in a complementary timescale, was affected by the single point mutations and to which extent it was similar to that found in similar organisms (11,14,44). Because the energy resolution allows probing motions in the picosecond range and the global diffusion of the whole cell does not contribute to the quasielastic width, it was not taken into account in the model. As detailed in the Supporting Materials and Methods, the data have been fitted with a single Lorentzian function and a δ function. Given the complexity of the biomolecules, the single Lorentzian provides an average indication of all active motions; therefore, only a qualitative and general comparison is possible. A typical example of data collected on the IN6 time-of-flight instrument is reported in Fig. S2.

Fig. 8 shows the full width at half maximum (FWHM) dependence on Q^2 at room temperature for the native (WT) and S264K, F265T, I163N mutants. We immediately observe two features: 1) all mutants share exactly the same Q^2 dependence and amplitude profile of the FWHM; and 2) the native sample retains the Q^2-dependence profile of the FWHM but with a reduced amplitude at large scale (low Q). A decrease of amplitude corresponds to a slowing down of the correlation time.

The observed $2\Gamma(Q)$ profile describes the existence of a diffusion in a confined space in the low Q^2 region coupled to a well-known jump diffusion behavior at the larger Q^2 values (short distance). In the low Q^2 region, the $2\Gamma_0(Q)$ is constant up to 0.77 $Å^{-1}$ for all samples, with a corresponding nonzero intercept equal to 0.2 meV for the WT and a nonzero intercept equal to 0.245 meV for the mutants.

Please cite this article in press as: Russo et al., Dynamics Properties of Photosynthetic Microorganisms Probed by Incoherent Neutron Scattering, Biophysical Journal (2019), https://doi.org/10.1016/j.bpj.2019.03.029

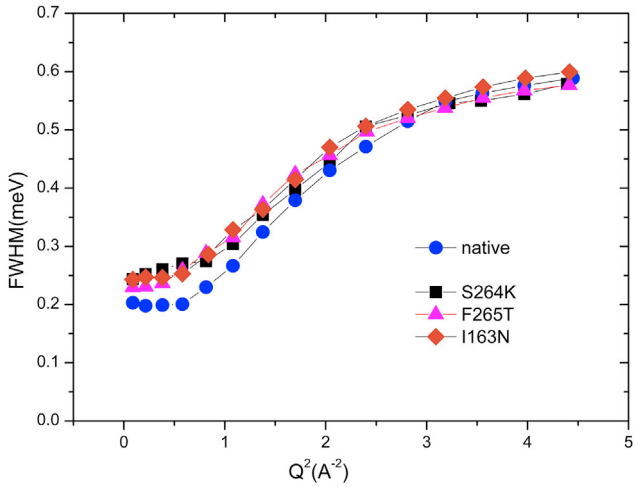

FIGURE 8 FWHM of the Lorentzian function plotted versus Q^2 for native *Chlamydomonas* and D1 mutants I163N, S264K, and F265T. To see this figure in color, go online.

Therefore, the corresponding correlation times are, respectively, ~6.5 ps for the native and 5.35 ps for the mutant cells. The presence of a plateau region is usually a fingerprint of constraint diffusions (geometrical constraints, local motions such as local rotations). Given the complexity of the system, we have taken into account the simplest model, which describes diffusion inside the volume of a sphere of radius a (45). The model gives access to the local diffusion coefficient and the size of the explored volume, which allows a simple comparison between the native green algae and the mutant's dynamics. In the Volino and Dianoux model (46), $2\Gamma_0(Q)$ is constant up to $Q_0 = \pi/a$ and it is equal to $(4.33*D)/a^2$, where a is the radius of the sphere where the diffusion D is the constraint. In this context, $a = 4$ Å and the diffusion coefficient is equal to 0.37 Å^2*meV (~$5.5*10^{-5}$ cm^2/s) for the native *Chlamydomonas* and 0.47 Å ^{2}*meV (~$7*10^{-5}$ cm^2/s) for the mutants.

An equivalent a value was also extracted from the analysis of the elastic incoherent structure factor as a function of Q (model and figure in Supporting Materials and Methods). The inferred a value is in agreement with the length scale explored by the motions in the *Escherichia coli* cell (46) and proteins in solutions and is slightly larger than hydrated powders and membrane proteins (~2 Å).

At larger Q^2 values (local dynamics) the general behavior could be analyzed with the jump diffusion model, which considers a residence time t_0 for one site before diffusing to another site (47). The diffusion coefficient would be slightly slower for the native cells. At high 2Γ (Q), all profiles approach a common plateau equal to 0.6 meV, which corresponds to a correlation time of ~2 ps.

In general, at large scale, the native photosynthetic cells show an internal dynamics slower than that of the I163N, F265T and S264K samples (i.e., both diffusion constants are slower than in the mutated organisms and the correlation times longer). The observed differences are very small; however, they are still significant if we take into account the similarity of the organism and high complexity of the cells.

To qualitatively confirm these results, we analyzed the experimental intermediate scattering function $I(Q,w)$ for two samples: WT and I163N (details in Supporting Materials and Methods).

We fit the time decay of $FH(Q,t)$ to a stretched exponential form, where deviations from $\beta = 1$ are signatures of a pronounced slowdown in dynamic processes with a characteristic relaxation time t, which is believed to be related to spatial heterogeneity in the dynamics.

The analysis with a stretched exponential confirmed important relaxation time dissimilarity at low Q values, where the native cells revealed a longer relaxation time compared to that of the I163N (Fig. 9 a). The β-exponent (Fig. 9 b), which represents the level of the dynamics heterogeneity, is Q dependent and it is slightly higher for the native *Chlamydomonas* cells. In both samples, the dynamics heterogeneity is more pronounced at low Q rather than at short scale where it approaches 0.8–0.9 values. A general relatively higher heterogeneity is observed in the I163N mutant (β-values are the same for all mutants). A pronounced dynamic heterogeneity, which translates to a higher variety

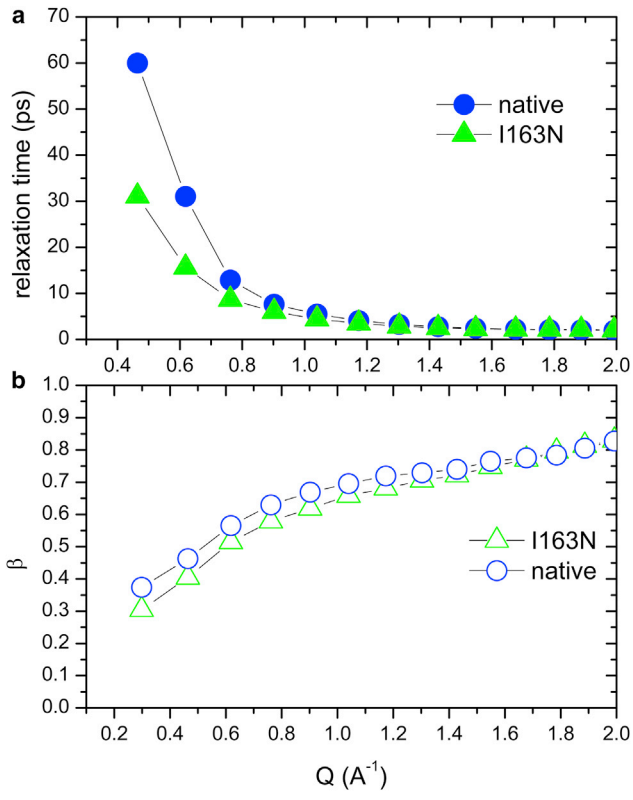

FIGURE 9 (*a*) Relaxation time and (*b*) stretched exponential parameter inferred from the fit to the intermediate scattering function at different Q values for native and I163N strains. To see this figure in color, go online.

Please cite this article in press as: Russo et al., Dynamics Properties of Photosynthetic Microorganisms Probed by Incoherent Neutron Scattering, Biophysical Journal (2019), https://doi.org/10.1016/j.bpj.2019.03.029

of active motions in the cell, could be related to dominant chemically heterogeneous environment. It was already observed that loss of distinct heterogeneity in the chemistry results in a dynamic signature that looks more like normal diffusion (48).

CONCLUSIONS

Probing the individual motions of hydrogen atoms, *EINS* and *QENS* techniques applied to living cells enabled us to characterize the active movements occurring in the different biomolecule conformations deriving from genetically or environmentally induced modifications of the native background. *QENS* and time-resolved laser-neutron (pump-probe) experiments have been performed intensively to study the dynamical properties of PSII-containing membranes isolated from spinach plants, revealing a temperature- and hydration-dependent dynamics controlling protein functionality (11–15). However, *EINS* and *QENS* studies on eukaryotic cells stably mutated in the photosynthetic RC have not been reported yet, and indeed, a few studies have been reported on in vivo whole cells because of their biological complexity (49–52).

Here, we provide evidence that mutants hosting single point mutations in the photosynthetic RC core proteins acquire more flexibility in terms of MSDs and relaxation time. Whereas in the nanosecond timescale, the degree of the observed flexibility is related to the mutation site, in the picosecond timescale, all mutants reveal the same dynamics. However, the relaxation dynamics, at the large length scale, is more affected than the local dynamics when compared to the native cells. We finally highlight the presence of a more pronounced dynamic heterogeneity in all mutants compared to the native cells, which could be related to a marked chemically heterogeneous environment.

We have also demonstrated by prompt fluorescence measurements of chlorophyll *a* in the S264K and F265T strains that a more flexible environment in the PQ-binding niche is associated to a less efficient ET from Q_A to Q_B. A similar function/dynamics relationship was also demonstrated in RCs of the purple bacteria *R. sphaeroides* trapped in active or inactive conformational intermediate states (frozen in the light or in the dark, respectively), indicating that flexibility at the quinones region plays a crucial role in evolutionarily distant organisms.

Indeed, the Q_A to Q_B ET in type II RCs is a well-known example of a temperature-dependent mechanism, guided by protein flexibility and transient conformational changes promoting electron gating and Q_B reduction and protonation (10,11,20,53,54).

We believe that the introduced mutations S264K and F265T impose new dynamics (more flexibility) perturbing the time evolution of conformational changes, breathing motions, and charge distributions occurring in the PSII complex during PQ-PQH_2 exchange mechanisms. Our hypothesis is supported by molecular dynamics simulations of the native PSII embedded in a phospholipid bilayer model in the presence of PQ or PQH_2 within the Q_B-binding site (34). The analyses, performed over a 50-ns simulation time, revealed that the release of PQH_2 is promoted by specific conformational changes, repulsive electrostatic interactions, and remodeling of the H-bond network occurring within a short region of the D1 protein shaping the walls of the binding pocket (residues 258–268). More specifically, the performed simulations indicated a pivotal role of the S264 and F265 residues in orchestrating the H-bond interactions with spatially neighboring D1 residues and in providing the physico-chemical properties underlying the intrinsic dynamics of the Q_B-binding pocket and PQ-PQH_2 exchange. Our work also provided experimental proof that disruption of this H-bond network in the D1 site-directed mutants S264K and F265T results in impairment of the Q_A-Q_B ET and also of the oxygen evolution rates (34,35). Hence, in these cases, more flexibility is associated to less functionality.

Instead, the intrinsically high flexibility measured in the I163N strain is not associated to a reduced efficiency of the ET rate, most likely because the mutation resides far from the PQ-binding niche. It is intriguing that at the physiological temperatures and in the nanosecond timescales, the I163N mutant shows the higher degree of flexibility compared to the other mutants. Moreover, in this mutant, inelastic coherent neutron scattering experiments revealed measurable alterations of the collective density fluctuations of hydrating water, indicating a higher flexibility compared to the native cells (55). Noteworthy, these features are associated to a radiation-tolerant phenotype able to maintain a high quantum yield of PSII photochemistry in extreme environmental conditions. Even if we cannot provide the molecular mechanisms underlying this stress tolerance yet, we can speculate that an increased flexibility could favor a remodeling of the multiscale and self-organizing intracellular assemblies whose hierarchical ordering is governed mainly by weak noncovalent interactions, optimizing the cell's functionality in stressful conditions.

Finally, beyond its crucial relevance to biology, a deep understanding of the structure/function/dynamics relationships of the photosynthetic complexes is expected to advance fundamental knowledge on atomic perturbations deriving by modifying the genetic background of living cells and to promote biotechnological innovations including the development of photoelectrochemical cells (56–58), biophotovoltaic systems (59–61), and biosensors (62–64).

SUPPORTING MATERIAL

Supporting Material can be found online at https://doi.org/10.1016/j.bpj.2019.03.029.

Please cite this article in press as: Russo et al., Dynamics Properties of Photosynthetic Microorganisms Probed by Incoherent Neutron Scattering, Biophysical Journal (2019), https://doi.org/10.1016/j.bpj.2019.03.029

AUTHOR CONTRIBUTIONS

D.R. planned and performed all the neutron scattering experiment, including data analysis and interpretation, and manuscript writing. M.D.L.: responsible for the physiological characterization of algae and preparation of samples for neutron scattering experiments. C.A.S. planned and performed neutron scattering experiment on RCs. P.S.: responsible for bacterial, RCs. G.R.: responsible for algae collection, preparation of samples for neutron scattering experiments, data interpretation, and manuscript writing.

ACKNOWLEDGMENTS

D.R. and G.R. thank ILL for beam time allocation and J. Ollivier, J. Combet, and B. Frick for their support using the IN6 and IN16 spectrometer. D.R. is grateful to J. Teixeira (Laboratoire Leon Brillouin, Commissariat Energie Atomique, France) for scientific discussion and suggestion and help during the IN6 experiment. P.S. and C.A.S. thank V. Derrien (Laboratoire de Chimie Phisique, Paris XI, France) for her contribution in the *R. sphaeroides* RC purification; D.R. and G.R. thank A. Antonacci, S. Pastorelli, and I. Husu (Istituto di Cristallografia, Consiglio Nazionale delle Ricerche, Italy) for help in *Chlamydomonas* samples preparation and U. Johanningmeier and I. Bertalan (Martin-Luther-Universität, Halle, Germany) for providing the D1 mutants. G.R. thanks the European Cooperation in Science and Technology Action TD1102 and the Lazio Regional Project (no. 85-2017-15256) for supporting the research activities.

REFERENCES

1. Smith, J. C., P. Tan, …, L. Hong. 2018. Dynamic neutron scattering by biological systems. *Annu. Rev. Biophys.* 47:335–354.
2. Peters, J., R. Prassl, and P. Oger. 2018. Probing the structure and dynamics of cells, cell components and endogenous nanoparticles under extreme conditions with neutrons. Biological, Physical and Technical Basics of Cell Engineering. Springer, pp. 401–420.
3. Tehei, M., and G. Zaccai. 2005. Adaptation to extreme environments: macromolecular dynamics in complex systems. *Biochim. Biophys. Acta.* 1724:404–410.
4. Tehei, M., D. Madern, …, G. Zaccai. 2001. Fast dynamics of halophilic malate dehydrogenase and BSA measured by neutron scattering under various solvent conditions influencing protein stability. *Proc. Natl. Acad. Sci. USA.* 98:14356–14361.
5. Doster, W., S. Cusack, and W. Petry. 1989. Dynamical transition of myoglobin revealed by inelastic neutron scattering. *Nature.* 337:754–756.
6. Peters, J., N. Martinez, …, F. Nachon. 2016. Dynamics of human acetylcholinesterase bound to non-covalent and covalent inhibitors shedding light on changes to the water network structure. *Phys. Chem. Chem. Phys.* 18:12992–13001.
7. Nickels, J. D., H. O'Neill, …, A. P. Sokolov. 2012. Dynamics of protein and its hydration water: neutron scattering studies on fully deuterated GFP. *Biophys. J.* 103:1566–1575.
8. Teixeira, J. 2009. Dynamics of hydration water in proteins. *Gen. Physiol. Biophys.* 28:168–173.
9. Combet, S., and J. M. Zanotti. 2012. Further evidence that interfacial water is the main "driving force" of protein dynamics: a neutron scattering study on perdeuterated C-phycocyanin. *Phys. Chem. Chem. Phys.* 14:4927–4934.
10. Sacquin-Mora, S., P. Sebban, …, C. Alba-Simionesco. 2007. Probing the flexibility of the bacterial reaction center: the wild-type protein is more rigid than two site-specific mutants. *Biochemistry.* 46:14960–14968.
11. Pieper, J., T. Hauss, …, G. Renger. 2007. Temperature- and hydration-dependent protein dynamics in photosystem II of green plants studied by quasielastic neutron scattering. *Biochemistry.* 46:11398–11409.
12. Pieper, J., T. Hauss, …, G. Renger. 2008. The effect of hydration on protein flexibility in photosystem II of green plants studied by quasielastic neutron scattering. *Eur. Biophys. J.* 37:657–663.
13. Pieper, J., and G. Renger. 2009. Flash-induced structural dynamics in photosystem II membrane fragments of green plants. *Biochemistry.* 48:6111–6115.
14. Pieper, J., M. Trapp, …, G. Renger. 2012. Temperature-dependent vibrational and conformational dynamics of photosystem II membrane fragments from spinach investigated by elastic and inelastic neutron scattering. *Biochim. Biophys. Acta.* 1817:1213–1219.
15. Nagy, G., J. Pieper, …, J. Peters. 2012. Dynamic properties of photosystem II membranes at physiological temperatures characterized by elastic incoherent neutron scattering. Increased flexibility associated with the inactivation of the oxygen evolving complex. *Photosynth. Res.* 111:113–124.
16. Michel, H., and J. Deisenhofer. 1988. Relevance of the photosynthetic reaction center from purple bacteria to the structure of photosystem II. *Biochemistry.* 27:1–7.
17. Cardona, T., J. W. Murray, and A. W. Rutherford. 2015. Origin and evolution of water oxidation before the last common ancestor of the cyanobacteria. *Mol. Biol. Evol.* 32:1310–1328.
18. Cardona, T., A. Sedoud, …, A. W. Rutherford. 1817. Charge separation in photosystem II: a comparative and evolutionary overview. *Biochim. Biophys. Acta.* 2012:26–43.
19. Graige, M. S., G. Feher, and M. Y. Okamura. 1998. Conformational gating of the electron transfer reaction QA-.QB–> QAQB-. in bacterial reaction centers of Rhodobacter sphaeroides determined by a driving force assay. *Proc. Natl. Acad. Sci. USA.* 95:11679–11684.
20. Shlyk, O., I. Samish, …, A. Scherz. 2017. A single residue controls electron transfer gating in photosynthetic reaction centers. *Sci. Rep.* 7:44580–44593.
21. Erickson, J. M., K. Pfister, …, J. D. Rochaix. 1989. Molecular and biophysical analysis of herbicide-resistant mutants of Chlamydomonas reinhardtii: structure-function relationship of the photosystem II D1 polypeptide. *Plant Cell.* 1:361–371.
22. Husu, I., G. Rodio, …, G. Rea. 2013. Insights into photo-electrochemical sensing of herbicides driven by Chlamydomonas reinhardtii cells. *Sens. Actuators B Chem.* 185:321–330.
23. Swainsbury, D. J., V. M. Friebe, …, M. R. Jones. 2014. Evaluation of a biohybrid photoelectrochemical cell employing the purple bacterial reaction centre as a biosensor for herbicides. *Biosens. Bioelectron.* 58:172–178.
24. Chatzipetrou, M., F. Milano, …, I. Zergioti. 2016. Functionalization of gold screen-printed electrodes with bacterial photosynthetic reaction centers by laser printing technology for mediatorless herbicide biosensing. *Electrochem. Commun.* 64:46–50.
25. Kleinfeld, D., M. Y. Okamura, and G. Feher. 1984. Electron-transfer kinetics in photosynthetic reaction centers cooled to cryogenic temperatures in the charge-separated state: evidence for light-induced structural changes. *Biochemistry.* 23:5780–5786.
26. Xu, Q., and M. R. Gunner. 2001. Trapping conformational intermediate states in the reaction center protein from photosynthetic bacteria. *Biochemistry.* 40:3232–3241.
27. Harris, E. H. 1989. The Chlamydomonas Sourcebook. A Comprehensive Guide to Biology and Laboratory UseVolume 1. Academic Press, San Antonio, CA.
28. Strasser, R. J., M. Srivastava, and M. Tsimilli. 2000. The fluorescence transient as a tool to characterize and screen photosynthetic samples. *In* Probing Photosynthesis: Mechanism, Regulation and Adaptation. M. Yunus, U. Pathre, and P. Mohanty, eds. Taylor and Francis, p. 445.
29. Chua, N. H., and P. Bennoun. 1975. Thylakoid membrane polypeptides of Chlamydomonas reinhardtii: wild-type and mutant strains deficient in photosystem II reaction center. *Proc. Natl. Acad. Sci. USA.* 72:2175–2179.

30. Rea, G., F. Polticelli, …, M. T. Giardi. 2009. Structure-based design of novel *Chlamydomonas reinhardtii* D1-D2 photosynthetic proteins for herbicide monitoring. *Protein Sci.* 18:2139–2151.
31. Rea, G., M. Lambreva, …, M. T. Giardi. 2011. Directed evolution and *in silico* analysis of reaction centre proteins reveal molecular signatures of photosynthesis adaptation to radiation pressure. *PLoS One.* 6:e16216.
32. Lambreva, M. D., D. Russo, …, G. Rea. 2014. Structure/function/dynamics of photosystem II plastoquinone binding sites. *Curr. Protein Pept. Sci.* 15:285–295.
33. Wilski, S., U. Johanningmeier, …, W. Oettmeier. 2006. Herbicide binding in various mutants of the photosystem II D1 protein of Chlamydomonas reinhardtii. *Pestic. Biochem. Physiol.* 84:157–164.
34. Zobnina, V., M. D. Lambreva, …, F. Polticelli. 2017. The plastoquinol-plastoquinone exchange mechanism in photosystem II: insight from molecular dynamics simulations. *Photosynth. Res.* 131:15–30.
35. Antonacci, A., M. D. Lambreva, …, G. Rea. 2018. Photosystem-II D1 protein mutants of Chlamydomonas reinhardtii in relation to metabolic rewiring and remodelling of H-bond network at Q_B site. *Sci. Rep.* 8:14745.
36. Vukich, M., P. L. Ganga, …, V. Zolesi. 2012. BIOKIS: a model payload for multidisciplinary experiments in microgravity. *Microgravity Sci. Technol.* 24:397–409.
37. Giardi, M. T., G. Rea, …, A. K. Mattoo. 2013. Mutations of photosystem II D1 protein that empower efficient phenotypes of Chlamydomonas reinhardtii under extreme environment in space. *PLoS One.* 8:e64352.
38. Johanningmeier, U., and S. Heiss. 1993. Construction of a Chlamydomonas reinhardtii mutant with an intronless *psbA* gene. *Plant Mol. Biol.* 22:91–99.
39. Umena, Y., K. Kawakami, …, N. Kamiya. 2011. Crystal structure of oxygen-evolving photosystem II at a resolution of 1.9 Å. *Nature.* 473:55–60.
40. Russo, D., M. A. Gonzalez, …, J. Teixeira. 2013. Evidence of dynamical constraints imposed by water organization around a bio-hydrophobic interface. *J. Phys. Chem. B.* 117:2829–2836.
41. Russo, D., M. Plazanet, …, T. Steinbach. 2016. Investigation into the relaxation dynamics of polymer-protein conjugates reveals surprising role of polymer solvation on inherent protein flexibility. *Biomacromolecules.* 17:141–147.
42. Tehei, M., B. Franzetti, …, G. Zaccai. 2004. Adaptation to extreme environments: macromolecular dynamics in bacteria compared in vivo by neutron scattering. *EMBO Rep.* 5:66–70.
43. Farhi, E., C. Rivasseau, …, A. Couté. 2008. Spectroscopic investigation of ionizing-radiation tolerance of a Chlorophyceae green microalga. *J. Phys. Condens. Matter.* 20:104216–104222.
44. Jasnin, M. 2009. Atomic-scale dynamics inside living cells explored by neutron scattering. *J. R. Soc. Interface.* 6 (*Suppl 5*):S611–S617.
45. Volino, F., and A. J. Dianoux. 1980. Neutron incoherent scattering law for diffusion in a potential of spherical symmetry: general formalism and application to diffusion inside a sphere. *Mol. Phys.* 41:271–279.
46. Jasnin, M., M. Moulin, …, M. Tehei. 2008. *In vivo* measurement of internal and global macromolecular motions in *Escherichia coli*. *Biophys. J.* 95:857–864.
47. Bée, M. 1988. Quasielastic Neutron Scattering: Principles and Applications in Solid State Chemistry, Biology and Materials Science. Adam Hilger, Bristol, England; Philadelphia.
48. Russo, D., R. K. Murarka, …, T. Head-Gordon. 2005. Molecular view of water dynamics near model peptides. *J. Phys. Chem. B.* 109:12966–12975.
49. Martinez, N., G. Michoud, …, J. Peters. 2016. High protein flexibility and reduced hydration water dynamics are key pressure adaptive strategies in prokaryotes. *Sci. Rep.* 6:32816.
50. Marty, V., M. Jasnin, …, B. Franzetti. 2013. Neutron scattering: a tool to detect *in vivo* thermal stress effects at the molecular dynamics level in micro-organisms. *J. R. Soc. Interface.* 10:20130003.
51. Anunciado, D. B., V. P. Nyugen, …, H. O'Neill. 2017. In vivo protein dynamics on the nanometer length scale and nanosecond time scale. *J. Phys. Chem. Lett.* 8:1899–1904.
52. Marques, M. P., A. L. Batista de Carvalho, …, L. A. Batista de Carvalho. 2017. Intracellular water - an overlooked drug target? Cisplatin impact in cancer cells probed by neutrons. *Phys. Chem. Chem. Phys.* 19:2702–2713.
53. Saito, K., A. W. Rutherford, and H. Ishikita. 2013. Mechanism of proton-coupled quinone reduction in photosystem II. *Proc. Natl. Acad. Sci. USA.* 110:954–959.
54. Kupitz, C., S. Basu, …, P. Fromme. 2014. Serial time-resolved crystallography of photosystem II using a femtosecond X-ray laser. *Nature.* 513:261–265.
55. Russo, D., G. Rea, …, G. Campi. 2016. Water collective dynamics in whole photosynthetic green algae as affected by protein single mutation. *J. Phys. Chem. Lett.* 7:2429–2433.
56. Mersch, D., C. Y. Lee, …, E. Reisner. 2015. Wiring of photosystem II to hydrogenase for photoelectrochemical water splitting. *J. Am. Chem. Soc.* 137:8541–8549.
57. Faccio, G., K. Gajda-Schrantz, …, A. Braun. 2015. Charge transfer between photosynthetic proteins and hematite in bio-hybrid photoelectrodes for solar water splitting cells. *Nano Converg.* 2:9.
58. Yaghoubi, H., E. Lafalce, …, A. Takshi. 2015. Large photocurrent response and external quantum efficiency in biophotoelectrochemical cells incorporating reaction center plus light harvesting complexes. *Biomacromolecules.* 16:1112–1118.
59. Kothe, T., N. Plumeré, …, W. Schuhmann. 2013. Combination of a photosystem 1-based photocathode and a photosystem 2-based photoanode to a Z-scheme mimic for biophotovoltaic applications. *Angew. Chem. Int.Engl.* 52:14233–14236.
60. Nguyen, K., and B. D. Bruce. 2014. Growing green electricity: progress and strategies for use of photosystem I for sustainable photovoltaic energy conversion. *Biochim. Biophys. Acta.* 1837:1553–1566.
61. Kazemzadeh, S., G. Riazi, and R. Ajeian. 2017. A novel approach of biophotovoltaic solid state solar cells based on a multilayer of PS1 complexes as active layer. *ACS Sustain. Chem. Eng.* 5:9836–9840.
62. Liu, Q., C. Wu, …, P. Wang. 2014. Cell-based biosensors and their application in biomedicine. *Chem. Rev.* 114:6423–6461.
63. Lim, J. W., D. Ha, …, T. Kim. 2015. Review of micro/nanotechnologies for microbial biosensors. *Front. Bioeng. Biotechnol.* 3:61.
64. Turemis, M., G. Rodio, …, M. T. Giardi. 2017. A novel optical/electrochemical biosensor for real time measurement of physiological effect of astaxanthin on algal photoprotection. *Sens. Actuators B Chem.* 241:993–1001.
65. Giardi, M. T., V. Scognamiglio, …, U. Johanningmeier. 2009. Optical biosensors for environmental monitoring based on computational and biotechnological tools for engineering the photosynthetic D1 protein of Chlamydomonas reinhardtii. *Biosens. Bioelectron.* 25:294–300.
66. Rea, G., F. Polticelli, …, M. T. Giardi. 2011. Computational biology, protein engineering, and biosensor technology: a close cooperation for herbicides monitoring. *In* Herbicides, Theory and Applications. S. Soloneski and M. L. Larramendy, eds. Intech Publishing, pp. 93–120.